THE JOURNAL OF PHYSICAL CHEMISTRY Letters

Letter

pubs.acs.org/JPCL

Investigating the Consistency of Models for Water Splitting Systems by Light and Voltage Modulated Techniques

Luca Bertoluzzi*,† and Juan Bisquert*,‡,§

†Department of Materials Science and Engineering, Stanford University, Stanford, California 94305, United States

‡Institute of Advanced Materials (INAM), Universitat Jaume I, 12006 Castelló, Spain

§Department of Chemistry, Faculty of Science, King Abdulaziz University, Jeddah 21589, Saudi Arabia

Supporting Information

ABSTRACT: The optimization of solar energy conversion devices relies on their accurate and nondestructive characterization. The small voltage perturbation techniques of impedance spectroscopy (IS) have proven to be very powerful to identify the main charge storage modes and charge transfer processes that control device operation. Here we establish the general connection between IS and light modulated techniques such as intensity modulated photocurrent (IMPS) and photovoltage spectroscopies (IMVS) for a general system that converts light to energy. We subsequently show how these techniques are related to the steady-state photocurrent and photovoltage and the external quantum efficiency. Finally, we express the IMPS and IMVS transfer functions in terms of the capacitive and resistive features of a general equivalent circuit of IS for the case of a photoanode used for solar fuel production. We critically discuss how much knowledge can be extracted from the combined use of those three techniques.

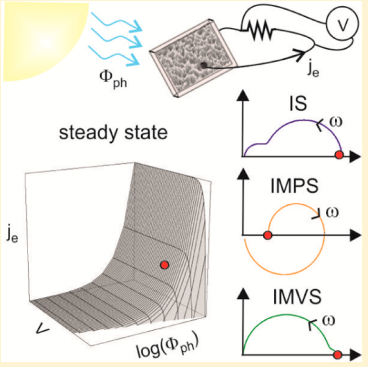

Analysis of solar energy conversion devices involves investigation of materials, interfaces, their combinations, and their performance and stability. A wide variety of materials and configurations have been investigated in the last few decades in the search for efficient and low-cost devices that can transform solar photons to useful energy. First, a number of new types of solar cells for the conversion of solar light to electricity emerged based on composites of absorbers and carrier transport phases, including nanostructured morphologies.[1] The most developed technologies are dye-sensitized solar cells, quantum dot solar cells, and bulk heterojunction organic solar cells. More recently, high-efficiency hybrid organic–inorganic perovskite solar cells that present a variety of intriguing and challenging properties vigorously emerged. Second, another important path of research for materials for clean energy production investigates the transformation of photons into a chemical fuel.[2] Although there are several alternative methods to reach such a goal,[3] the use of a semiconductor that performs light absorption and photo-induced catalytic surface reactions in photoelectrochemical applications has been at the center of the research of many laboratories in recent decades, and this area has been especially active over the last 10 years.

Investigating new materials, interfaces, and devices requires suitable characterization methods that provide knowledge about the mechanisms of operation, performance, and stability of the suggested configurations. In this work, we focus on the small-frequency modulated techniques that emerged first in electrochemistry and then were extended to a wide range of studies of solar energy conversion devices. In order to establish the scope of our discussion, we present in Figure 1 a scheme that represents the basic mechanism of operation of the devices that convert light to energy. The light absorber film of macroscopic area A and thickness d is supplemented with selective contacts that extract the electrical current density, j_e, which is delivered to an external circuit for electricity production or to a solution for the formation of chemical fuels. The voltage and electrical current are measured at the contacts of the device. We describe the incident radiation normal to the electrode surface with a monochromatic photon flux $\Phi_{ph}(\lambda)$ for optical wavelength λ, and we express this quantity in units of electrical current density, $j_\Phi = q\Phi_{ph}(\lambda)$, where q is the elementary charge.

The idealized model of Figure 1 provides a good representation of the main device configuration used to investigate the development of materials and devices for solar energy conversion, although more advanced concepts such as photonic full spectrum utilization are neglected. The performance of all such devices can be characterized by a relationship between three variables, namely, the electrical current density, j_e, the voltage, V, and the illumination current intensity, j_Φ. We will assume that a stabilized steady-state performance has been achieved, implying that the characteristics do not evolve with time. In the case of solar fuel conversion, we assume the absence of parasitic reactions so that j_e provides the rate of fuel formation. In these conditions, the current density–voltage curve at a given level of illumination, also known as the

Received: November 20, 2016
Accepted: December 13, 2016
Published: December 13, 2016

DOI: 10.1021/acs.jpclett.6b02714
J. Phys. Chem. Lett. 2017, 8, 172–180

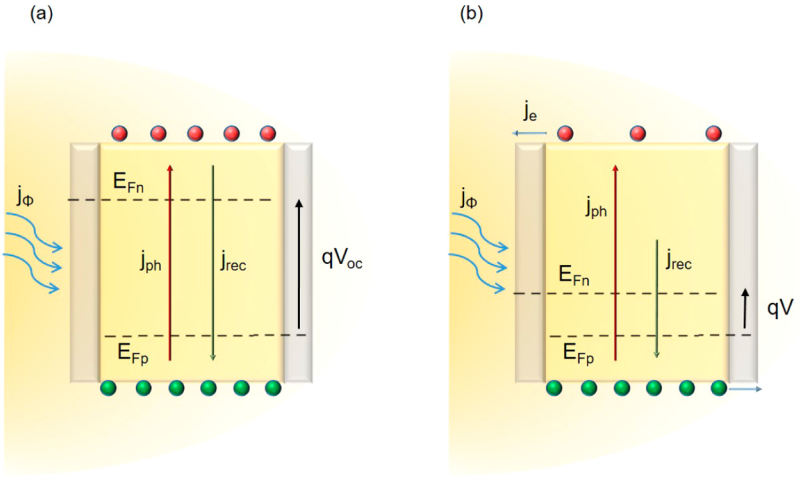

Figure 1. Fundamental energy diagram of a solar cell showing the band edges for electrons and holes (thin lines), the Fermi levels (dashed lines), and the selective contacts. The current is extracted only at the contacts via the free carriers thermalized in the band edges. We assume low device thickness that results in homogeneous light absorption and high carrier mobilities, and we neglect surface recombination, which implies that the Fermi levels are flat. V is the applied voltage, j_e is the external electrical current density, j_Φ is the incident photon flux in units of electrical current, $j_{ph} = Q_\Phi j_\Phi$ (where Q_Φ is the external quantum efficiency) is the short-circuit photocurrent, and j_{ph}/q is also the carrier flux internally generated by the optical radiation. j_{rec}/q is the internal recombination flux. For clarity, j_0/q, the carrier flux internally generated by the absorption of blackbody radiation is not represented. (a) Open-circuit condition V_{oc} is the photovoltage; (b) electrical current generation at $V < V_{oc}$.

polarization curve, is the central characteristic that determines the power conversion efficiency of the device at steady-state operation. Also important are the curves obtained in open-circuit ($j_e = 0$) and short-circuit ($V = 0$) conditions, as discussed later. The stabilized light surface of operation points, or the Λ_0 surface for brevity, shown in Figure 2, can be

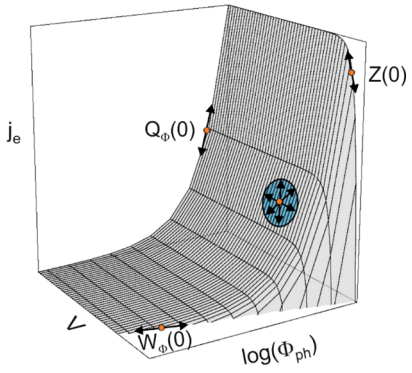

Figure 2. Steady-state performance of a solar energy conversion device, the light Λ_0 surface in terms of electrical current j_e, voltage V, and illumination flux Φ_{ph}. When these variables are taken in pairs, the slope of the curve is given by the zero frequency value of the transfer functions. In the figure, slopes are shown in the main 2D planes, but the same analysis can be performed at any point of the surface (when the three variables are not zero), as indicated by the circular tangent plane.

determined by a time-independent functional model of the physical variables as follows

$$\Lambda_0(j_e, V, j_\Phi) = 0 \tag{1}$$

However, such a steady-state surface in the (j_e, V, j_Φ) space does not contain detailed mechanistic information, and it is necessary to work in the dynamic regime, using methods such as small perturbation modulated techniques. The rationale for these latter techniques is to perform additional experiments at one selected point of the Λ_0 surface involving small perturbation of the variables and measuring the resulting output. The angular frequency of the perturbation ω is varied over a broad range of values corresponding to frequencies from mHz to MHz. Under time variation, the frequency analyzer instrument produces stabilized output at the given angular frequency. The state of the system will then be represented by a more general function Λ_ω that reduces to eq 1 when $\omega = 0$ (the steady-state limit of operation). From the standpoint of modeling, Λ_ω is obtained by a set of drift−diffusion equations involving small perturbation of carrier densities that can be solved in terms of ($\hat{j}_e$, $\hat{V}$, $\hat{j}_\Phi$).[4] The use of a small perturbation ensures a linear response so that, in contrast to eq 1, the modulated variables (denoted by a circumflex) obey a linear relationship

$$\left(\frac{\partial \Lambda_\omega}{\partial j_e}\right)\hat{j}_e + \left(\frac{\partial \Lambda_\omega}{\partial j_\Phi}\right)\hat{j}_\Phi + \left(\frac{\partial \Lambda_\omega}{\partial V}\right)\hat{V} = 0 \tag{2}$$

When the variables are taken in pairs of output/input, the result of the frequency modulated spectroscopies is a transfer function that allows the identification of resistances and capacitances in the operational response. This procedure can be repeated along a selected trajectory on the Λ_0 surface. The dependence of parameters on the steady-state characteristics can be investigated by the different techniques described here, removing any ambiguity in the model characteristics.

The most widely used technique is the modulation of current with respect to voltage, which gives an electrical impedance. This traditional method is known as impedance spectroscopy (IS), and it is widely used in several classes of solar energy devices.[5,6] In addition, one can also modulate the light variable and relate it either to modulated current or voltage. These techniques are rather interesting because the light produces the primary excitation from which energy must flow out of the device. These methods are termed intensity modulated photocurrent spectroscopy (IMPS) and intensity modulated photovoltage spectroscopy (IMVS). IMPS was largely developed by Laurie Peter and his co-workers in connection with the operation of the planar semiconductor−electrolyte

DOI: 10.1021/acs.jpclett.6b02714
J. Phys. Chem. Lett. 2017, 8, 172−180

interface.[7,8] Later on, the technique became important for the analysis of carrier transport in extended mesoporous films and dye-sensitized solar cells.[9,10] IMVS was developed as a tool to investigate recombination mechanisms in dye-sensitized solar cells.[11,12] Recently, these methods were applied to water oxidation in hematite photoelectrodes[13,14] and perovskite solar cells.[15,16] Here, we will not present an account of the historical evolution of these methods and their many ramifications. Surveys of the recent literature have recently been published.[17,18]

In the past, there has been an asymmetry of analysis that complicated the consistent validation of detailed models. While IS is traditionally studied in terms of the convenient tool of equivalent circuits (ECs),[6,19,20] the analysis of IMPS and IMVS has been very focused on the comparison of kinetic time constants to evaluate the competition of carrier recombination and extraction.[14,21−23] Kinetic time constants have the general form of a product of resistance by capacitance: $k = (RC)^{-1}$. A central feature of frequency modulated spectroscopies is that they provide simultaneous in-phase and out-of-phase response; hence, they allow us to separately visualize the variation of both resistances and capacitances along a Λ_0 trajectory. We remark that the analysis of time constants can be especially complex in the case of multilayer devices that demand the identification of specific sites for voltage and charge accumulation.[24] The combination of IS, IMPS, and IMVS provides a potential powerful tool for a direct analytical description by identification of charge storage modes via system capacitances in addition to charge transfer by resistance components, provided that the different experimental methods of analysis are effectively combined in a single framework. The relevant time constants in the system can also be evaluated by time domain methods such as transient photoinduced absorption spectroscopy, which must be correlated to the frequency domain techniques;[25,26] however, this topic is out of the scope of this work.

The connection of the results of the various frequency methods in specific systems has been the topic of several studies over the last decades.[17,27,28] Recently, Halme[17] showed the relation of the different methods in an investigation of dye-sensitized solar cells. In this work, we aim to present a broader unified approach for a general reference system as that in Figure 1. We establish the meaning of the transfer functions at very low frequency, which recovers essential quantities for steady-state performance such as dc resistance or the external quantum efficiency dependence on photon flux. On the basis of the general insight obtained for the reference system, we develop more complex models associated with water splitting reaction steps at the semiconductor surface. We study the distinction of models for photooxidation of water via direct and indirect hole transfer at the semiconductor surface that have been described previously for IS,[29] and we show the parameters and spectral shapes of the different transfer functions. Thus, this work will provide a sound basis for the validation of physical models from independent measurements that must converge into a single picture.

Steady-State Operation Model. We describe specific Λ_0 surface performance for the model of Figure 1. The rate of generation of carriers, integrated over the whole film, has the value

$$G = a(\lambda)\Phi_{ph}(\lambda) \tag{3}$$

in terms of the spectral absorptance $a(\lambda)$. The external photocurrent at short circuit relates to the generation rate by means of the internal quantum efficiency η_{IQE}

$$j_{ph} = j_e(V = 0) = q\eta_{IQE}a(\lambda)\Phi_{ph}(\lambda) \tag{4}$$

or, in other terms

$$\eta_{EQE} = \frac{j_{ph}}{j_\Phi} \tag{5}$$

where $\eta_{EQE}(\lambda) = \eta_{IQE}(\lambda)a(\lambda)$ is the steady-state external quantum efficiency. In the weak absorption limit, $a(\lambda) = \alpha(\lambda)d$ for the absorption coefficient $\alpha(\lambda)$. In detailed modeling, one may consider additional photonic features of the device. It is important to realize that $\eta_{EQE}(\lambda)$ is a function of the steady-state illumination, and in fact, the measurement of $\eta_{EQE}(\lambda,\Phi_{ph})$ constitutes an important tool for investigation of the characteristics of dye-sensitized solar cells[30] and the mechanisms of photoinduced oxidation of electrolyte species at semiconductor electrodes.[31]

The characteristic current density−voltage curve for the fundamental model of a solar cell is based on the balance equation that can be inferred from Figure 1b

$$j_e = j_{ph} - j_0(e^{qV/mk_BT} - 1) \tag{6}$$

Here, k_BT is the thermal energy. The recombination rate is determined by j_0, the reverse saturation current, which is also the parameter for recombination in forward mode, and a diode ideality factor m. The parentheses in eq 6 express detailed balance equilibrium in the dark. The diode equation model in eq 6 determines the Λ_0 surface shown in Figure 2. Provided that $j_{ph} \gg j_0$, the open-circuit photovoltage has the expression

$$V_{oc} = \frac{mk_BT}{q}\ln\left(\frac{j_{ph}}{j_0}\right) \tag{7}$$

In terms of the incident photon flux, we have

$$V_{oc} = \frac{mk_BT}{q}\ln(\Phi_{ph}) + \frac{mk_BT}{q}\ln\left(\frac{q\eta_{EQE}}{j_0}\right) \tag{8}$$

Definition of the Transfer Functions. Let us now consider the result of the measurement of modulated small perturbations. To this end, we rewrite eq 2 using coefficients that are the transfer functions corresponding to the measurement of only two modulation variables, in different combinations. Here, we present a notation that makes a direct connection with quantities of interest in steady-state performance, as discussed later on. We have

$$\hat{j}_e = Q_\Phi(\omega)\hat{j}_\Phi + Z^{-1}(\omega)\hat{V} \tag{9}$$

The impedance is defined in the absence of modulated illumination as

$$Z(\omega) = -\frac{\left(\frac{\partial\Lambda_\omega}{\partial j_e}\right)_{\hat{j}_\Phi=0}}{\left(\frac{\partial\Lambda_\omega}{\partial V}\right)_{\hat{j}_\Phi=0}} = \left.\frac{\hat{V}(\omega)}{\hat{j}_e(\omega)}\right|_{\hat{j}_\Phi=0} \tag{10}$$

With IMPS, we impose $\hat{V} = 0$ and the resulting photocurrent modulation $\hat{j}_e(\omega)$ is measured. The corresponding transfer function is the modulated quantum yield

DOI: 10.1021/acs.jpclett.6b02714
J. Phys. Chem. Lett. 2017, 8, 172−180

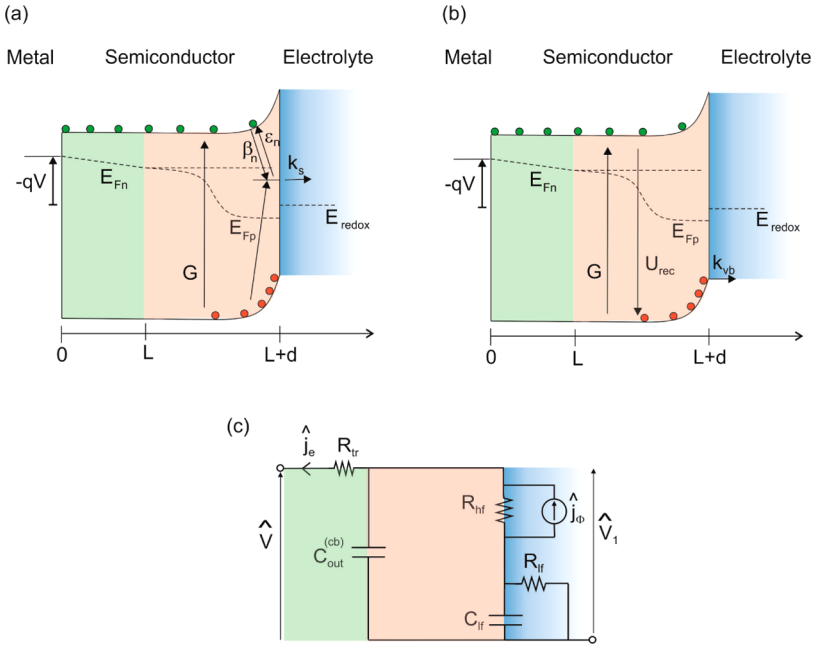

Figure 3. (a) Indirect charge transfer model for solar fuel production by a photoanode of length $L + d$. Electrons and holes are photogenerated at a rate G. Electrons can be trapped (kinetic constant: β_n) and detrapped (ε_n) in surface states at the semiconductor/electrolyte interface. All of the photogenerated holes are trapped and can either recombine with trapped electrons or be transferred at a rate k_s to the redox couple in solution with energy E_{redox}. The concentration of free electrons and holes follows the quasi-Fermi levels, E_{Fn} and E_{Fp}. At the metal/semiconductor interface, E_{Fn} is directly modulated by the applied voltage V. (b) Direct charge transfer model. Photogenerated holes can either recombine with electrons at a rate U_{rec} or be transferred to the electrolyte from the valence band at a rate k_{vb}. (c) General EC for both models, calculated for a small perturbation of light intensity ($\hat{\Phi}$) and a small perturbation of voltage ($\hat{V}$). The small perturbation of light intensity is modeled by a current source. Note that the voltage perturbation can arise from the light intensity perturbation, as for IMVS, or can be imposed electrically, as for IS. In those circuits, R_{tr} is the transport resistance, $C_{out}^{(cb)}$ is the outer capacitance of the conduction band, R_{lf} and C_{lf} are the low-frequency resistance and capacitance, and R_{hf} is the high-frequency resistance. Each of these electrical elements is expressed in Supporting Information (SI) in terms of the kinetic parameters and steady-state concentrations specific to each model.

$$Q_\Phi(\omega) = -\frac{\left(\frac{\partial \Lambda_\omega}{\partial j_\Phi}\right)_{\hat{V}=0}}{\left(\frac{\partial \Lambda_\omega}{\partial j_e}\right)_{\hat{V}=0}} = \left.\frac{\hat{j}_e(\omega)}{\hat{j}_\Phi(\omega)}\right|_{\hat{V}=0} \tag{11}$$

Finally, IMVS consists of maintaining the photocurrent perturbation at zero ($\hat{j}_e = 0$) and measuring the corresponding photovoltage perturbation. In this case, the transfer function reads

$$W_\Phi(\omega) = -\frac{\left(\frac{\partial \Lambda_\omega}{\partial j_\Phi}\right)_{\hat{j}_e=0}}{\left(\frac{\partial \Lambda_\omega}{\partial V}\right)_{\hat{j}_e=0}} = \left.\frac{\hat{V}(\omega)}{\hat{j}_\Phi(\omega)}\right|_{\hat{j}_e=0} \tag{12}$$

For a given steady state, the impedance of the system can be directly expressed in terms of the IMVS and IMPS transfer functions as

$$Z(\omega) = \frac{W_\Phi(\omega)}{Q_\Phi(\omega)} \tag{13}$$

While eqs 10−13 were suggested by Halme[17] for dye-sensitized solar cells, eq 9 derived from eq 2 constitutes an important and novel equation. These are the general expressions, which must be satisfied for any small perturbation of light and voltage and at any frequency, unlike eqs 10−13, which are valid for one type of perturbation only. Note that as defined here $Z(\omega)$ and $W_\Phi(\omega)$ have units of $\Omega{\cdot}cm^2$, while $Q_\Phi(\omega)$ is dimensionless.

Interpretation of the Transfer Functions at Zero Frequency. As mentioned before, the modulated transfer functions provide us detailed spectral information involving resistive and capacitive behavior at a given point on the stabilized Λ_0 surface. One particular important result is the limit of the transfer function at $\omega = 0$. At this frequency, the transient (capacitive) signal vanishes while the steady-state one remains. Therefore, the transfer function in this limit is directly connected to a small perturbation of the steady-state curve. This analysis is well-known for the impedance function. The quotient of the small quantities at low frequency has the value

$$Z(0) = \frac{\hat{V}(0)}{\hat{j}_e(0)} \tag{14}$$

Therefore, we obtain a resistance $Z(0) = R_{dc}$ given by

$$R_{dc} = \left(\frac{\partial j_e}{\partial V}\right)^{-1} \tag{15}$$

The dc resistance of the photoelectrode R_{dc} (per unit area) is the reciprocal of the slope of the $j_e{-}V$ curve, and this provides an essential validation method for comparing IS and stationary measurement.[19] Importantly, this observation allows the reconstruction of the $j_e{-}V$ curve from the fundamental processes determined by IS.[32,33]

Next, we analyze the section $j_e{-}j_\Phi$ of the Λ_0 surface at $V = 0$. From eq 11, we have the limit at low frequency

DOI: 10.1021/acs.jpclett.6b02714
J. Phys. Chem. Lett. 2017, 8, 172−180

$$Q_\Phi(0) = \frac{\hat{j}_e(0)}{q\hat{\Phi}_{ph}(0)} = \frac{\partial j_{ph}}{\partial j_\Phi} \tag{16}$$

Comparing eqs 16 and 5, we note that $Q_\Phi(0)$ is the slope of η_{EQE} dependence on the photon flux Φ_{ph}. This property has been discussed by Vanmaekelbergh et al.[10,34] for nanoporous semiconductor electrodes.

Finally, we address the curve V_{oc}–j_Φ on the Λ_0 surface at $j_e = 0$. This curve has often been measured in order to determine recombination properties of dye-sensitized solar cells[11,35] and perovskite solar cells.[36] It is usually presented as V_{oc} vs log Φ_{ph} due to the standard relation in eq 8. The transfer function has the low-frequency value

$$W_\Phi(0) = \frac{\hat{V}(0)}{q\hat{\Phi}(0)} = \frac{1}{q}\frac{\partial V_{oc}}{\partial \Phi_{ph}} \tag{17}$$

or else

$$W_\Phi(0) = \frac{1}{q\Phi_{ph}}\frac{\partial V_{oc}}{\partial \ln \Phi_{ph}} \tag{18}$$

According to the model of eq 6,we obtain

$$\frac{\partial V_{oc}}{\partial \ln \Phi_{ph}} = \frac{mk_BT}{q} \tag{19}$$

Therefore, the function $W_\Phi(0)$ at low frequency is related to the derivative of the function V_{oc} vs log Φ_{ph}, which gives information on recombination in the solar cell, as discussed by Huang et al.[11]

Models for Photo-oxidation at the Semiconductor Surface. We now apply the previous general considerations to the models for light-to-fuel conversion at the semiconductor electrode. We consider here the case of a photoanode. In the context of the operation of the photoelectrochemical cell, it is very important to establish the main pathway for the transfer of photogenerated holes, either by direct transfer from the valence band or by indirect transfer via surface states. The models are shown in Figure 3. Previously, the features of IS have been described in detail,[6,29] and here, we express the IMPS and IMVS responses in terms of the resistances and chemical capacitances associated with each charge storage mode. We remark that the quantity $Q_\Phi(0)$ was analyzed by steady-state methods by Salvador and co-workers, and they established markedly different dependences for both types of charge transfer mechanisms.[31]

We model the semiconductor/electrolyte system with a thin homogeneous semiconductor layer of thickness $L + d$. On the left ($x = 0$), the semiconductor is contacted by an ohmic electron-selective contact. The semiconductor/electrolyte interface ($x = L + d$) is a blocking layer for electrons. The important feature of this model is that the hole density cannot be modulated by external voltage, unlike in the model of Figure 1, but only by light due to the step of the hole Fermi level at the interface, which is a rather fundamental feature of this type of system, as described by Salvador.[37] In contrast, the homogeneous concentration of electrons in the conduction band is directly modulated by the voltage V as

$$n = n_0 \exp\left(-\frac{qV}{k_BT}\right) \tag{20}$$

The index 0 refers to an equilibrium quantity. In addition, transport of electrons may be limited by low bulk conductivity, modeled by the transport resistance, R_{tr}, which implies a voltage drop

$$V_1 = V - R_{tr}j_e \tag{21}$$

hence

$$Z(\omega) = \frac{\hat{V}}{\hat{j}_e} = R_{tr} + Z_1(\omega) \tag{22}$$

where Z_1 corresponds to the internal EC of the semiconductor electrode.

Upon illumination, n free electrons and p free holes per unit volume are generated at a rate G, defined by eq 3. In the indirect charge transfer model (Figure 3a), the p_s photogenerated holes per unit volume are trapped in a density of surface states N_{ss} and can either recombine with the trapped electrons or be transferred to the electrolyte for fuel production with rate constant k_s. In the direct model (Figure 3b), free holes can recombine with free electrons via a band-to-band recombination mechanism or can be directly transferred to the electrolyte via the valence band with the rate constant k_{vb}. The continuity equation for electrons reads

$$\frac{\partial n}{\partial t} = \frac{1}{q}\frac{\partial j_e}{\partial x} + \frac{\partial p_s}{\partial t} + k_s(p_s - p_{s0}) + \frac{\partial p}{\partial t} + k_{vb}(p - p_0) \tag{23}$$

In the case of the indirect charge transfer model, $k_{vb} = 0$, $p = p_0$, $\partial p/\partial t = 0$, and p_s is governed by the equation

$$\frac{\partial p_s}{\partial t} = G - \beta_n n p_s + \varepsilon_n(N_{ss} - p_s) - k_s(p_s - p_{s0}) \tag{24}$$

where β_n and ε_n are the electron trapping and detrapping rates, respectively. On the contrary, for the direct charge transfer model, $k_s = 0$, $\partial p_s/\partial t = 0$, the bimolecular recombination rate is B, and p is determined by the rate equation

$$\frac{\partial p}{\partial t} = G - B(np - n_0p_0) - k_{vb}(p - p_0) \tag{25}$$

The general expression for the concomitant direct and indirect charge transfer processes has been treated in ref 20.

Determination of the Transfer Functions. To obtain the transfer functions associated with the IS, IMPS, and IMVS techniques, one can apply a small sinusoidal perturbation of light intensity, which directly modulates the generation rate ($\hat{G} = \alpha(\lambda)\hat{\Phi}_{ph}(\lambda)$) in the rate eqs 24 and 25. The corresponding voltage ($\hat{V}$) and current ($\hat{j}_e$) perturbations are obtained by linearizing and applying the Laplace transform to eqs 20 and 23–25. After integration over the homogeneous semiconductor layer of length d, we obtained

$$\hat{n} = -\frac{q\hat{V}_1}{k_BT}\overline{n} \tag{26}$$

$$i\omega\hat{n} = -\frac{\hat{j}_e}{qd} + (i\omega + k_s)\hat{p}_s + (i\omega + k_{vb})\hat{p} \tag{27}$$

$$\hat{p}_s = \frac{\hat{G} - \beta_n\overline{p}_s\hat{n}}{i\omega + \beta_n\overline{n} + \varepsilon_n + k_s} \tag{28}$$

$$\hat{p} = \frac{\hat{G} - B\overline{p}\,\hat{n}}{i\omega + B\overline{n} + k_{vb}} \tag{29}$$

DOI: 10.1021/acs.jpclett.6b02714
J. Phys. Chem. Lett. 2017, 8, 172–180

where $\bar{x}$ refers to a steady-state quantity. Note that eq 28 is valid only for the indirect charge transfer model (i.e., when $\hat{p} = 0$), while eq 29 is valid for the direct one (i.e., when $\hat{p}_s = 0$). The steady-state hole concentrations ($\bar{p}_s$ and $\bar{p}$) are obtained by setting the time derivative to zero in eqs 24 and 25 and are given in the SI. The photocurrent perturbation for the indirect charge transfer model is then obtained by combining eqs 26−28

$$\hat{j}_e = \frac{q^2 d}{k_B T}\bar{n}\left(i\omega + \frac{(i\omega + k_s)\beta_n \bar{p}_s}{i\omega + \beta_n \bar{n} + \varepsilon_n + k_s}\right)\hat{V}_1 + \frac{\alpha(\lambda) d(i\omega + k_s)}{i\omega + \beta_n \bar{n} + \varepsilon_n + k_s}\hat{j}_\Phi \quad (30)$$

The photocurrent corresponding to the direct charge transfer model is obtained by combining eqs 26, 27, and 29

$$\hat{j}_e = \frac{q^2 d}{k_B T}\bar{n}\left(i\omega + \frac{(i\omega + k_{vb})B\bar{p}}{i\omega + B\bar{n} + k_{vb}}\right)\hat{V}_1 + \frac{\alpha(\lambda) d(i\omega + k_{vb})}{i\omega + B\bar{n} + k_{vb}}\hat{j}_\Phi \quad (31)$$

Equations 30 and 31 clearly illustrate the important connection between photocurrent, (photo)voltage, and photogeneration, provided by eq 9. Given the similar form of these equations, one can express the photocurrent for both models of Figure 3a,b with one single equation

$$\hat{j}_e = \left(i\omega C_\mu^{cb} + \frac{1}{R_{hf} + \frac{1}{(R_{lf})^{-1} + i\omega C_{lf}}}\right)\hat{V}_1 + \frac{Q_0}{1 + \frac{R_{lf}}{R_{hf}}\frac{1}{1 + i\omega C_{lf} R_{lf}}}\hat{j}_\Phi \quad (32)$$

In eq 32, $Q_0 = \alpha(\lambda)d$, C_μ^{cb} is the conduction band capacitance, C_{lf} and R_{lf} are, respectively, the low-frequency capacitance and resistance, and R_{hf} is the high-frequency resistance. The expressions of those elements are specified for each model of Figure 3a,b in the SI. Equation 32, combined with eq 22, allows one to extract the general transfer functions for both models

$$Z_1(\omega) = \left[i\omega C_\mu^{cb} + \frac{1}{R_{hf} + Z_{lf}(\omega)}\right]^{-1} \quad (33)$$

$$Z_{lf}(\omega) = [(R_{lf})^{-1} + i\omega C_{lf}]^{-1} \quad (34)$$

$$Q_\Phi(\omega) = Q_0\left[\left(1 + \frac{R_{tr}}{Z_1(\omega)}\right)\left(1 + \frac{Z_{lf}(\omega)}{R_{hf}}\right)\right]^{-1} \quad (35)$$

$$W_\Phi(\omega) = Q_0 Z_1(\omega)\left(1 + \frac{Z_{lf}(\omega)}{R_{hf}}\right)^{-1} \quad (36)$$

Models Characteristics. The general EC corresponding to IS, IMPS, and IMVS can be obtained from the analytical models described above, and it is shown in Figure 3c. We remark that C_μ^{cb} has been replaced by a more general capacitance, the outer capacitance of the conduction band C_{out}^{cb}, which accounts for displacement currents such as charging of the Helmholtz layer, typically described as a capacitor C_H.[38] It can be noted that light modulation introduces a current source to the classical EC obtained with IS, which arises from the generation term in eq 28 and 29.

If $R_{tr} = 0$, the contribution from the chemical capacitance of the conduction band (contained in $Z_1(\omega)$) cannot be observed in the IMPS response. On the contrary, $W_\Phi(\omega)$ is independent of the transport resistance because for IMVS the current passing through R_{tr} is zero. Obviously, IMPS is better suited to observe phenomena that take place in series with the generation step, like electron transport, while IMVS captures the parallel component that often contains recombination phenomena. This is why IMPS was measured predominantly at short circuit and IMVS at open circuit in solar cells.[34,39] However, as remarked by Halme,[17] the measurements can be taken at any point of the Λ_0 surface.

We now explain which features can be extracted from the typical patterns displayed in Figure 4 with the IS, IMPS, and

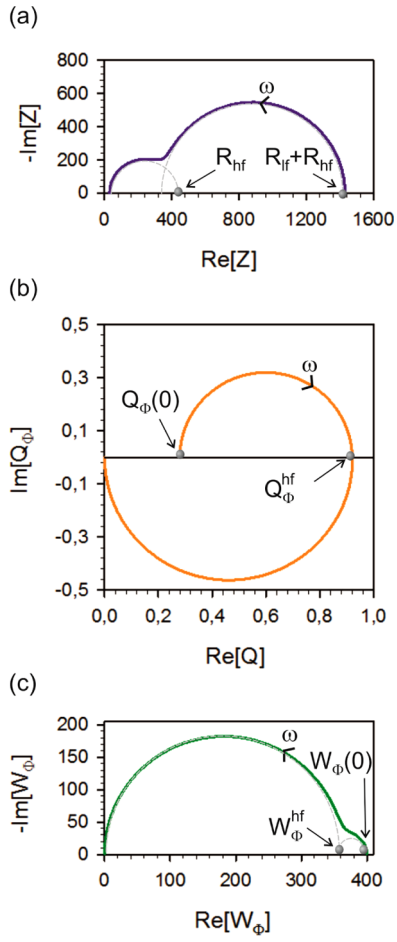

Figure 4. Simulation of the (a) IS, (b) IMPS, and (c) IMVS responses calculated for the following resistance and capacitance values, R_{tr} = 30 Ω·cm^2, R_{lf} = 1 kΩ·cm^2, R_{hf} = 0.4 kΩ·cm^2, C_{lf} = 10 μF/cm^2, and C_{out}^{cb} = 1 μF/cm^2, and Q_0 = 1.

IMVS techniques. In particular, we discuss the typical case in which two semicircles can be detected by IS (Figure 4a), which corresponds to the situation in which $C_{out}^{cb} \ll C_{lf}$. (The opposite situation would lead to one single arc, and only limited kinetic information would be extracted.) This case has been well established in the investigation of hematite photoelectrodes by IS.[19,40−43] The C_{out}^{cb} is attributed to the combination of dielectric capacitances such as the depletion layer and C_H, while the low-frequency capacitance is often associated with the storage of charge at surface states or catalytic layers,[44] that is, the low-frequency arc is regulated by the low-frequency capacitance, C_{lf}, and the low-frequency resistance, R_{lf}. The latter corresponds to the diameter of the low frequency semicircle. Therefore, this arc gives information about the main

DOI: 10.1021/acs.jpclett.6b02714
J. Phys. Chem. Lett. 2017, 8, 172−180

hole storage mode (via C_{lf}) and the hole transfer process (via R_{lf}). On the contrary, the high-frequency arc is regulated by C_{out}^{cb} and R_{hf} and gives information about the population of electrons in the conduction band as well as the main electron recombination pathway. The ratio of both resistances (R_{hf}/R_{lf}) has been shown to play an important role because it controls the onset photovoltage and photocurrent at small applied bias.[20]

The corresponding IMPS pattern is displayed in Figure 4b. Note that the IMPS frequency dependence is inverted with respect to the one of IS because $Z \propto 1/\hat{j}_e$ while $Q_\Phi \propto \hat{j}_e$. The low-frequency arc observed in IMPS is also controlled by C_{lf}, while the high-frequency one is controlled by C_{out}^{cb}. The radii of both arcs depend on all resistances involved in the model. In fact, both intersections with the real axis, shown in Figure 4b, can be calculated within the approximation $C_{out}^{cb} \ll C_{lf}$, and they have the value

$$Q_\Phi(0) = Q_0 \frac{R_{hf}}{R_{tr} + R_{hf} + R_{lf}} \tag{37}$$

$$Q_\Phi^{hf} = Q_0 \frac{R_{hf}}{R_{tr} + R_{hf}} \tag{38}$$

From eqs 37 and 38, one can recover the ratio R_{hf}/R_{lf} previously mentioned for the IS analysis of the main limiting mechanism of solar fuel production at small applied bias.

Finally, the IMVS pattern simulated in Figure 4c shows two contributions. Both arcs contain the contributions of both low- and high-frequency capacitances, unlike for IS and IMPS. In fact, assuming $C_{out}^{cb} \ll C_{lf}$, one can calculate the intersections with the real axis displayed in Figure 4c

$$W_\Phi(0) = Q_0 R_{hf} \tag{39}$$

$$W_\Phi^{hf} = \frac{C_{lf}}{C_{out}^{cb} + C_{lf}} Q_0 R_{hf} \tag{40}$$

Equations 37−40 obtained above are similar to the those published by Peter and co-workers and Schefold and co-workers.[21,27] Yet, in those models, charge transfer is modulated by the Helmholtz capacitance, which is included in our model within the outer capacitance of the conduction band, C_{out}^{cb}, and is independent of the charge storage mode (surface states or valence band). Unlike these models, our model allows identification of the main charge transfer mechanism through the voltage variations of the low-frequency capacitance. In addition, it allows estimation of the surface concentration of trapped/free holes in addition to the charge transfer kinetics.[29]

Having completed study of the information that the three modulated techniques provides for the same model system, we now remark that light modulated techniques do not give more information than the electrical impedance technique itself. This observation may appear surprising because one may expect that different types of perturbation will modulate different processes. For instance, voltage does not generate minority carriers, while illumination does, and one would aim to extract different information with light modulated techniques than with IS. However, the information that can be extracted from these techniques is conveyed by one single carrier, independently of the type of perturbation that is applied. In the n-type semiconductors discussed here, the information is contained in the variations of the electron quasi-Fermi level. In other words, whether light or voltage perturbation is applied, one will only be able to detect the processes that induce electron Fermi level variations. The holes can only be detected through their recombination with electrons. As a matter of fact, if holes were not recombining with electrons, one would not be able to detect them with light/voltage modulated techniques. This shows that light modulated techniques can provide only as much information as IS. This conclusion was previously remarked by Vanmaekelbergh et al. for recombination in semiconductor electrodes.[4] One should however notice that each process will be detected at different frequencies, depending on the nature of the technique. Hence, processes that occur at frequencies too low/high to be detected by IS may be detected by light modulated techniques.

In summary, we have established the connection between light intensity, voltage, and electrical current modulation techniques through a general formalism involving a stabilized Λ_0 surface describing steady-state performance. The photocurrent arising from a small perturbation of light and/or voltage can be expressed as a linear combination of the IS and IMPS (or IMVS) transfer functions. This relation is of high interest because it allows one to connect the transfer function of light intensity modulated techniques to physical quantities of fundamental importance obtained by IS, such as the chemical capacitance, the recombination resistance, and/or the charge transfer resistance. Hence, unlike a purely kinetic treatment, this method allows identification of the main charge storage mode(s) of a system at a given illumination and voltage. We calculated the IMPS and IMVS transfer functions of a photoanode used for solar fuel production for two distinct types of charge transfer: indirect charge transfer from the surface states and direct charge transfer from the valence band. We have provided expressions of the transfer functions in terms of the chemical capacitance of the surface states/valence band, the trapping−detrapping/recombination resistance, and the charge transfer resistance from the surface states/valence band. We showed that the EC for light intensity modulated techniques is the same as the one of IS with the additional contribution of a current source, which models light modulation. Finally, we explained how to recover the capacitive and resistive features from the complex plane plots for IMPS and IMVS, in relation with IS. Therefore, we have built a unified background for the analysis of solar devices with small light and voltage perturbation techniques, which should have profound impact in terms of device characterization and optimization.

■ ASSOCIATED CONTENT

Supporting Information

The Supporting Information is available free of charge on the ACS Publications website at DOI: 10.1021/acs.jpclett.6b02714.

Steady-state concentration of free and trapped holes and expressions of the circuital elements of Figure 3c of the main text (PDF)

■ AUTHOR INFORMATION

Corresponding Authors

*E-mail: bertoluz@stanford.edu (L.B.).

*E-mail: bisquert@uji.es (J.B.).

ORCID

Juan Bisquert: 0000-0003-4987-4887

Notes

The authors declare no competing financial interest.

DOI: 10.1021/acs.jpclett.6b02714
J. Phys. Chem. Lett. 2017, 8, 172−180

■ ACKNOWLEDGMENTS

We acknowledge funding from MINECO of Spain under Project MAT2013-47192-C3-1-R and Generalitat Valenciana Project PROMETEOII/2014/020.

■ REFERENCES

(1) O'Regan, B.; Moser, J.; Anderson, M.; Grätzel, M. Vectorial electron injection into transparent semiconductor membranes and electric field effects on the dynamics of light-induced charge separation. *J. Phys. Chem.* **1990**, *94*, 8720−8726.
(2) Gimenez, S.; Bisquert, J. *Photoelectrochemical Solar Fuel Production. From Basic Principles to Advanced Devices*; Springer, 2016.
(3) Nielander, A. C.; Shaner, M. R.; Papadantonakis, K. M.; Francis, S. A.; Lewis, N. S. A taxonomy for solar fuels generators. *Energy Environ. Sci.* **2015**, *8*, 16−25.
(4) Vanmaekelbergh, D.; de Wit, A. R.; Cardon, F. Recombination in semiconductor electrodes: Investigation by the electrical and optoelectrical impedance method. *J. Appl. Phys.* **1993**, *73*, 5049−5057.
(5) Fabregat-Santiago, F.; Garcia-Belmonte, G.; Mora-Seró, I.; Bisquert, J. Characterization of nanostructured hybrid and organic solar cells by impedance spectroscopy. *Phys. Chem. Chem. Phys.* **2011**, *13*, 9083−9118.
(6) Bisquert, J.; Gimenez, S.; Bertoluzzi, L.; Herraiz-Cardona, I. Analysis of photelectrochemical systems by Impedance Spectroscopy. In *Photoelectrochemical Solar Fuel Production. From Basic Principles to Advanced Devices*; Gimenez, S., Bisquert, J., Eds.; Springer, 2016.
(7) Li, J.; Peat, R.; Peter, L. M. Surface recombination at semiconductor electrodes. Part II. Photoinduced "near-surface" recombination centres in p-GaP. *J. Electroanal. Chem. Interfacial Electrochem.* **1984**, *165*, 41.
(8) Peter, L. M. Dynamic aspects of semiconductor photoelectrochemistry. *Chem. Rev.* **1990**, *90*, 753−769.
(9) Dloczik, L.; Ileperuma, O.; Lauermann, I.; Peter, L. M.; Ponomarev, E. A.; Redmond, G.; Shaw, N. J.; Uhlendorf, I. Dynamic response of dye-sensitized nanocrystalline solar cells: Characterization by Intensity-Modulated Photocurrent Spectroscopy. *J. Phys. Chem. B* **1997**, *101*, 10281−10289.
(10) de Jongh, P. E.; Vanmaekelbergh, D. Trap-limited electronic transport in assemblies of nanometer-size TiO_2 Particles. *Phys. Rev. Lett.* **1996**, *77*, 3427−3430.
(11) Huang, S. Y.; Schlichthörl, G.; Nozik, A. J.; Grätzel, M.; Frank, A. J. Charge recombination in dye-sensitized nanocrystallyne TiO_2 solar cells. *J. Phys. Chem. B* **1997**, *101*, 2576−2582.
(12) Schlichthörl, G.; Huang, S. Y.; Sprague, J.; Frank, A. J. Band edge movement and recombination kinetics in dye-sensitized nanocrystalline TiO_2 solar cells: a study by Intensity Modulated Photovoltage Spectroscopy. *J. Phys. Chem. B* **1997**, *101*, 8141−8155.
(13) Cachet, H.; Sutter, E. M. M. Kinetics of water oxidation at TiO_2 nanotube arrays at different pH domains investigated by electrochemical and light-modulated Impedance Spectroscopy. *J. Phys. Chem. C* **2015**, *119*, 25548−25558.
(14) Thorne, J. E.; Jang, J.-W.; Liu, E. Y.; Wang, D. Understanding the origin of photoelectrode performance enhancement by probing surface kinetics. *Chem. Sci.* **2016**, *7*, 3347−3354.
(15) Todinova, A.; Idígoras, J.; Salado, M.; Kazim, S.; Anta, J. A. Universal features of electron dynamics in solar cells with TiO_2 contact: From dye solar cells to perovskite solar cells. *J. Phys. Chem. Lett.* **2015**, *6*, 3923−3930.
(16) Contreras, L.; Idigoras, J.; Todinova, A.; Salado, M.; Kazim, S.; Ahmad, S.; Anta, J. A. Specific cation interactions as the cause of slow dynamics and hysteresis in dye and perovskite solar cells: a small-perturbation study. *Phys. Chem. Chem. Phys.* **2016**, *18*, 31033−31042.
(17) Halme, J. Linking optical and electrical small amplitude perturbation techniques for dynamic performance characterization of dye solar cells. *Phys. Chem. Chem. Phys.* **2011**, *13*, 12435−12446.
(18) Klotz, D.; Ellis, D. S.; Dotan, H.; Rothschild, A. Empirical in operando analysis of the charge carrier dynamics in hematite photoanodes by PEIS, IMPS and IMVS. *Phys. Chem. Chem. Phys.* **2016**, *18*, 23438−23457.
(19) Klahr, B.; Gimenez, S.; Fabregat-Santiago, F.; Hamann, T.; Bisquert, J. Water oxidation at hematite photoelectrodes: The role of surface states. *J. Am. Chem. Soc.* **2012**, *134*, 4294−4302.
(20) Bertoluzzi, L.; Bisquert, J. Equivalent circuit of electrons and holes in thin semiconductor films for photoelectrochemical water splitting applications. *J. Phys. Chem. Lett.* **2012**, *3*, 2517−2522.
(21) Ponomarev, E. A.; Peter, L. M. A generalized theory of intensity modulated photocurrent spectroscopy (IMPS). *J. Electroanal. Chem.* **1995**, *396*, 219.
(22) Wijayanthaa, K. G. U.; Saremi-Yarahmadi, S.; Peter, L. M. Kinetics of oxygen evolution at a-Fe_2O_3 photoanodes: a study by photoelectrochemical impedance spectroscopy. *Phys. Chem. Chem. Phys.* **2011**, *13*, 5264−5270.
(23) Peter, L. M. Energetics and kinetics of light-driven oxygen evolution at semiconductor electrodes: the example of hematite. *J. Solid State Electrochem.* **2013**, *17*, 315−326.
(24) Nellist, M. R.; Laskowski, F. A. L.; Lin, F.; Mills, T. J.; Boettcher, S. W. Semiconductor−electrocatalyst interfaces: Theory, experiment, and applications in photoelectrochemical water splitting. *Acc. Chem. Res.* **2016**, *49*, 733−740.
(25) Le Formal, F.; Pendlebury, S. R.; Cornuz, M.; Tilley, S. D.; Grätzel, M.; Durrant, J. R. Back electron−hole recombination in hematite photoanodes for water splitting. *J. Am. Chem. Soc.* **2014**, *136* (6), 2564−2574.
(26) Ma, Y.; Kafizas, A.; Pendlebury, S. R.; Le Formal, F.; Durrant, J. R. Photoinduced absorption spectroscopy of CoPi on $BiVO_4$: The function of CoPi during water oxidation. *Adv. Funct. Mater.* **2016**, *26* (27), 4951−4960.
(27) Schefold, J. Impedance and intensity modulated photocurrent spectroscopy as complementary differential methods in photoelectrochemistry. *J. Electroanal. Chem.* **1992**, *341* (1), 111−136.
(28) Ponomarev, E. A.; Peter, L. M. A comparison of intensity modulated photocurrent spectroscopy and photoelectrochemical impedance spectroscopy in a study of photoelectrochemical hydrogen evolution at p-InP. *J. Electroanal. Chem.* **1995**, *397*, 45−52.
(29) Bertoluzzi, L.; Lopez-Varo, P.; Jimenez Tejada, J. A.; Bisquert, J. Charge transfer processes at the semiconductor/electrolyte interface for solar fuel production: insight from impedance spectroscopy. *J. Mater. Chem. A* **2016**, *4*, 2873−2879.
(30) Jennings, J. R.; Li, F.; Wang, Q. Reliable determination of electron diffusion length and charge separation efficiency in dye-sensitized solar cells. *J. Phys. Chem. C* **2010**, *114*, 14665−14674.
(31) Mora-Seró, I.; Villarreal, T. L.; Bisquert, J.; Pitarch, A.; Gómez, R.; Salvador, P. Photoelectrochemical behavior of nanostructured TiO_2 thin film electrodes in contact with aqueous electrolytes containing dissolved pollutants: a model for distinguishing between direct and indirect interfacial hole transfer from photocurrent measurements. *J. Phys. Chem. B* **2005**, *109*, 3371−3380.
(32) Boix, P. P.; Guerrero, A.; Marchesi, L. F.; Garcia-Belmonte, G.; Bisquert, J. Current-voltage characteristics of bulk heterojunction organic solar cells: Connection between light and dark curves. *Adv. En. Mater.* **2011**, *1*, 1073−1078.
(33) Raga, S. R.; Fabregat-Santiago, F. Temperature effects in dye-sensitized solar cells. *Phys. Chem. Chem. Phys.* **2013**, *15*, 2328−2336.
(34) de Jongh, P. E.; Vanmaekelbergh, D. Investigation of the electronic properties of nanocrystalline particulate TiO_2 electrodes by intensity-modulated photocurrent spectroscopy. *J. Phys. Chem. B* **1997**, *101*, 2716−2722.
(35) Bisquert, J.; Zaban, A.; Salvador, P. Analysis of the mechanism of electron recombination in nanoporous TiO_2 dye-sensitized solar cells. Nonequilibrium steady state statistics and transfer rate of electrons in surface states. *J. Phys. Chem. B* **2002**, *106*, 8774−8782.
(36) Gouda, L.; Gottesman, R.; Ginsburg, A.; Keller, D. A.; Haltzi, E.; Hu, J.; Tirosh, S.; Anderson, A. Y.; Zaban, A.; Boix, P. P. Open circuit potential build-up in perovskite solar cells from dark conditions to 1 sun. *J. Phys. Chem. Lett.* **2015**, *6*, 4640−4645.

DOI: 10.1021/acs.jpclett.6b02714
J. Phys. Chem. Lett. 2017, 8, 172−180

(37) Salvador, P. Semiconductors' photoelectrochemistry: A kinetic and termodynamic analysis in the light of equilibrium and non-equilibrium models. *J. Phys. Chem. B* **2001**, *105*, 6128−6141.
(38) Schefold, J. Charge transfer at photoelectrochemical solar cells: conclusions from the open-circuit impedance of p-InP in $V^{3+/2+}$. *J. Electrochem. Soc.* **1995**, *142*, 850−862.
(39) Wang, H.; Peter, L. M. A Comparison of different methods to determine the electron diffusion length in dye-sensitized solar cells. *J. Phys. Chem. C* **2009**, *113*, 18125−18133.
(40) Iandolo, B.; Hellman, A. The role of surface states in the oxygen evolution reaction on hematite. *Angew. Chem., Int. Ed.* **2014**, *53* (49), 13404−13408.
(41) Klahr, B.; Hamann, T. Water oxidation on hematite photo-electrodes: insight into the nature of surface states through in situ spectroelectrochemistry. *J. Phys. Chem. C* **2014**, *118*, 10393−10399.
(42) Chou, J.-C.; Lin, S.-A.; Lee, C.-Y.; Gan, J.-Y. Effect of bulk doping and surface-trapped states on water splitting with hematite photoanodes. *J. Mater. Chem. A* **2013**, *1*, 5908−5914.
(43) Monllor-Satoca, D.; Bartsch, M.; Fabrega, C.; Genc, A.; Reinhard, S.; Andreu, T.; Arbiol, J.; Niederberger, M.; Morante, J. R. What do you do, titanium? Insight into the role of titanium oxide as a water oxidation promoter in hematite-based photoanodes. *Energy Environ. Sci.* **2015**, *8*, 3242−3254.
(44) Klahr, B.; Gimenez, S.; Fabregat-Santiago, F.; Hamann, T.; Bisquert, J. Photoelectrochemical and impedance spectroscopic investigation of water oxidation with "Co-Pi" coated hematite electrodes. *J. Am. Chem. Soc.* **2012**, *134*, 16693−16700.

DOI: 10.1021/acs.jpclett.6b02714
J. Phys. Chem. Lett. 2017, 8, 172−180